Nucl. Fusion **49** (2009) 065012 (15pp) doi:10.1088/0029-5515/49/6/065012

Principal physics developments evaluated in the ITER design review

R.J. Hawryluk[1], D.J. Campbell[2], G. Janeschitz[2], P.R. Thomas[3], R. Albanese[4], R. Ambrosino[4], C. Bachmann[2], L. Baylor[5], M. Becoulet[6], I. Benfatto[2], J. Bialek[7], A. Boozer[7], A. Brooks[1], R. Budny[1], T. Casper[8], M. Cavinato[2], J.-J. Cordier[2], V. Chuyanov[2], E. Doyle[9], T. Evans[10], G. Federici[11], M. Fenstermacher[8], H. Fujieda[12], K. G'al[13], A. Garofalo[10], L. Garzotti[14], D. Gates[1], Y. Gribov[2], P. Heitzenroeder[1], T.C. Hender[14], N. Holtkamp[2], D. Humphreys[10], I. Hutchinson[15], K. Ioki[2], J. Johner[6], G. Johnson[2], Y. Kamada[12], A. Kavin[16], C. Kessel[1], R. Khayrutdinov[17], G. Kramer[1], A. Kukushkin[2], K. Lackner[18], I. Landman[19], P. Lang[14], Y. Liang[20], J. Linke[20], B. Lipschultz[15], A. Loarte[2], G.D. Loesser[1], C. Lowry[2], T. Luce[10], V. Lukash[17], S. Maruyama[2], M. Mattei[21], J. Menard[1], M. Merola[2], A. Mineev[16], N. Mitchell[2], E. Nardon[14], R. Nazikian[1], B. Nelson[5], C. Neumeyer[1], J.-K. Park[1], R. Pearce[2], R.A. Pitts[2], A. Polevoi[2], A. Portone[3], M. Okabayashi[1], P.H. Rebut[2], V. Riccardo[14], J. Roth[18], S. Sabbagh[7], G. Saibene[3], G. Sannazzaro[2], M. Schaffer[10], M. Shimada[2], A. Sen[22], A. Sips[18], C.H. Skinner[1], P. Snyder[10], R. Stambaugh[10], E. Strait[10], M. Sugihara[2], E. Tsitrone[6], J. Urano[12], M. Valovic[14], M. Wade[10], J. Wesley[10], R. White[1], D.G. Whyte[15], S. Wu[2], M. Wykes[2] and L. Zakharov[1]

[1] Princeton Plasma Physics Laboratory, PO Box 451, Princeton, NJ 08543, USA
[2] ITER Organization, CS 90 046, F-13067 Saint Paul lez Durance Cedex, France
[3] Fusion for Energy Joint Undertaking, Josep Pla 2, Torres Diagonal Litoral - B3, 08019 Barcelona, Spain
[4] Association Euratom-ENEA-CREATE, Univ. Napoli Federico II, Via Claudio 21, I-80125 Napoli, Italy
[5] Oak Ridge National Laboratory, Oak Ridge, TN 37831, USA
[6] Association EURATOM-CEA Cadarache, F-13108 St Paul lez Durance, France
[7] Department of Applied Physics and Applied Mathematics, Columbia University, New York, NY, USA
[8] Lawrence Livermore National Laboratory, Livermore, CA 94551, USA
[9] Department of Electrical Engineering and PSTI, University of California, Los Angeles, CA, USA
[10] General Atomics, San Diego, CA 92186-5608, USA
[11] European Fusion Development Agreement Close Support Unit – Garching, Boltzmannstrasse 2, D-85748 Garching bei Munchen, Germany
[12] Japan Atomic Energy Agency, Naka, Ibaraki-ken 311-0193, Japan
[13] KFKI RMKI, EURATOM Association, POB 49, H-1525 Budapest, Hungary
[14] EURATOM/UKAEA Fusion Association, Culham Science Centre, Abingdon, Oxon OX14 3DB, UK
[15] Massachusetts Institute of Technology, Plasma Science and Fusion Center, Cambridge, MA 02139, USA
[16] DV Efremov Scientific Research Institute of Electrophysical Apparatus, St Petersburg 196641, Russian Federation
[17] Troitsk Institute for Innovation and Fusion Research, Troitsk, Russian Federation
[18] Max-Planck-Institut für Plasmaphysik, EURATOM Association, Boltzmannstrasse 2, D-85748 Garching bei München, Germany
[19] Forschungszentrum Karlsruhe, Institute for Pulsed Power and Microwave Technology, PO Box 3640, 76021 Karlsruhe, Germany
[20] Forschungszentrum Jülich GmbH, Association EURATOM-FZ Jülich, Institut für Plasmaphysik, Trilateral Euregio Cluster, D-52425 Jülich, Germany
[21] Association Euratom-ENEA-CREATE, Univ. Mediterranea, Loc. Feo di Vito, I-89060 RC, Italy
[22] Institute for Plasma Research, Gandhinagar, India

Received 30 December 2008, accepted for publication 14 April 2009
Published 7 May 2009
Online at stacks.iop.org/NF/49/065012

Abstract
As part of the ITER Design Review and in response to the issues identified by the Science and Technology Advisory Committee, the ITER physics requirements were reviewed and as appropriate updated. The focus of this paper will be on recent work affecting the ITER design with special emphasis on topics affecting near-term procurement

arrangements. This paper will describe results on: design sensitivity studies, poloidal field coil requirements, vertical stability, effect of toroidal field ripple on thermal confinement, material choice and heat load requirements for plasma-facing components, edge localized modes control, resistive wall mode control, disruptions and disruption mitigation.

PACS numbers: 28.52.−s, 52.55.−s, 52.35.Py, 52.40.Hf, 52.55.Fa, 52.55.Rk, 52.55.Tn

1. Introduction

The goal of ITER is to demonstrate the scientific and technological feasibility of fusion power for peaceful purposes [1]. As part of the ITER Design Review [2] and in response to the issues identified by the Science and Technology Advisory Committee (STAC), the ITER physics requirements were reviewed and as appropriate updated. This entailed applying the results described in the special issue of *Nuclear Fusion* on 'Progress in the ITER Physics Basis' [1], performing new analyses and conducting experiments on the major tokamak devices to ensure that the ITER design is consistent with current understanding. This was a worldwide effort, with major contributions from the ITPA, which were reported, in part, at the 2008 IAEA Fusion Energy Conference. Much of the work discussed in this paper was presented to the ITER STAC, who provided detailed comments. A comprehensive review of all of the scientific and technical issues will not be attempted. Instead, the focus will be on recent work affecting the ITER design with special emphasis on topics affecting near-term procurement arrangements.

A key programmatic goal for ITER is that 'The device should achieve extended burn in inductively driven plasmas with the ratio of fusion power to auxiliary heating power, Q, of at least 10 ($Q \geqslant 10$) ...' [1]. The focus on this goal during the Design Review was motivated by the need to finalize the specifications for the toroidal field coil [3] and vacuum vessel procurement arrangements as well as submitting the documentation for licensing [4], which are on the critical path to completing the construction project. Areas requiring additional research will be discussed.

2. Design sensitivity studies

'Progress in the ITER Physics Basis' [5] provides an extensive review of the empirical scaling projections as well as one-dimensional modelling assessments for ITER. The physics uncertainties in projecting the performance of ITER are addressed assuming that the machine operates at full design parameters. The impact of modest changes in machine parameters, B_t, I_p and κ ($\pm 10\%$) on the fusion power and Q were evaluated with the HELIOS code (an earlier version of the code is described in [6]) as well as by spreadsheet analysis. The energy confinement time projections are based on the empirical scaling [1]

$$\tau_{E,th}^{IPB98(y,2)} = 0.0562 H_{IPB98(y,2)} I_p^{0.93} B_T^{0.15} \bar{n}_e^{0.41} \times P^{-0.69} R^{1.97} M^{0.19} \kappa_a^{0.78} \varepsilon^{0.58},$$

where the units are s, MA, T, $10^{19}\,\mathrm{m}^{-3}$, MW, m and amu, respectively, ε is the aspect ratio, a/R, and the elongation, κ_a, is defined as $\kappa_a = S_o/(\pi a^2)$, with S_o being the plasma cross-section. $H_{IPB98(y,2)}$ denotes a constant normally taken to be unity.

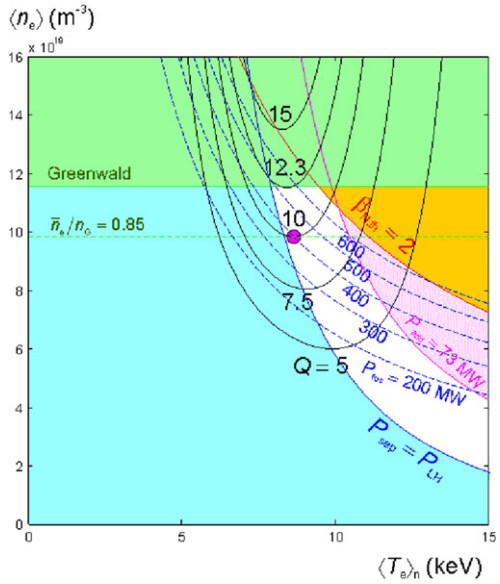

Figure 1. The operating space is shown on the basis of calculations using the HELIOS code for the baseline 15 MA, 5.3 T ELMy H-mode scenario. For reference, the baseline heating power is 73 MW. At an operating density of 0.85 of the Greenwald limit, the projected Q is 10 with 40 MW of heating power and $\tau_E = 3.8$ s The accessible operating regime in white is bounded by the estimated power required to achieve an H-mode, the Greenwald density and the available auxiliary heating power.

As shown in figure 1, the maximum operating density, auxiliary heating power and the criteria to achieve H-mode confinement defines the operating space for the baseline 15 MA, 5.3 T scenario. To avoid the degradation in confinement at high density, the operating density is assumed to be 0.85 of the Greenwald density limit. The baseline heating power is 73 MW and could be further increased if necessary. The back transition from H-mode to L-mode confinement is assumed to occur at the same power as the L- to H-mode transition at the same parameters. The analysis by Martin *et al* [7] taking into account the effective mass of the plasma is used to calculate the power threshold for H-mode confinement. At the nominal $Q = 10$ operating point, the power threshold is ~70 MW and the power through the separatrix ~79 MW, taking into account an estimate for the radiated power. In a burning plasma, bremsstrahlung and synchrotron radiation are more important than in current experiments. Thus, bremsstrahlung and synchrotron radiated power as well as an estimate for line radiation within the separatrix were subtracted out, which may be a conservative assumption since that was not

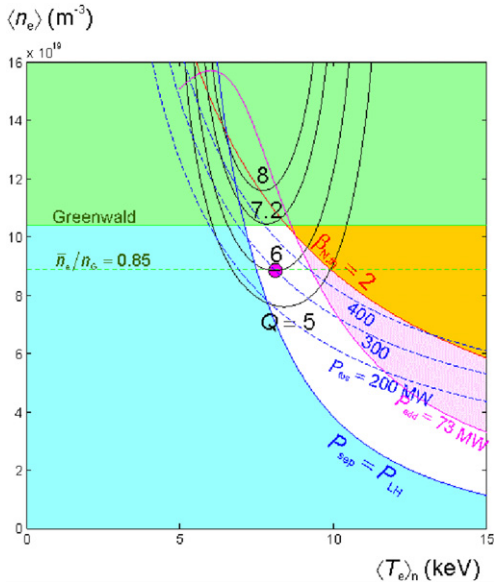

Figure 2. Operating scenario assuming a 10% reduction in toroidal field (4.77 T) and plasma current (13.5 MA) relative to figure 1. For the nominal operating point at 0.85 of the Greenwald density, $Q \sim 6$ and $\tau_E = 3.3$ s.

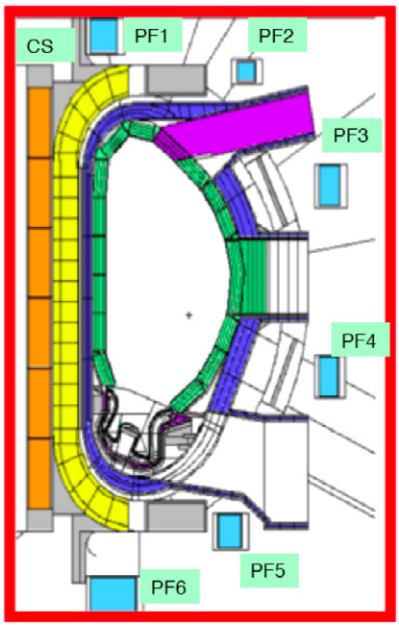

Figure 3. The poloidal field system of ITER is depicted. 'CS' refers to the central solenoid, which consists of six segments and provides predominantly, but not solely, the magnetic flux swing required for inductive current drive, while the six poloidal field ('PF') coils make the major contribution to plasma shaping and active control.

done in the development of the power threshold database. The uncertainty in the power threshold for the H-mode transition [5, 7, 8] and the possible occurrence of Type III ELMs near the power threshold [9], which degrades energy confinement, motivates further research.

As indicated in figure 1, operation at high density approaching the Greenwald limit is advantageous. Relative to current experiments, ITER will rely on pellet fuelling, which may enable higher density operation and more peaked density profiles, which are also advantageous. Recent experiments on ASDEX Upgrade and JET have shown the density profile becomes more peaked with decreasing plasma collisionality, which is characteristic of ITER operation ([5] and references therein).

For constant values of the safety factor, a 10% reduction in the toroidal field and plasma current as shown in figure 2 results in Q being reduced from ~10 to ~6. Similarly, if the elongation were reduced by ~10% and the current decreased to maintain the safety factor at the baseline level, then Q is also reduced to ~6. Alternatively, when the current is increased from 15 to 17 MA, the value of Q is projected to increase to ~20. While operation at 17 MA is not a baseline operating point, it will be assessed during the design of ITER. Due to the increased likelihood of disruptions and increased forces and potential for damage due to disruptions, the implications of operating at 17 MA will be evaluated during the hydrogen-commissioning phase.

These sensitivity studies indicate the value of operational ranges with improved energy confinement, and research is on-going to identify such operating modes. Recent results from ASDEX Upgrade, DIII-D, JET and JT-60U, using the hybrid regime in which the $q(0) \sim 1$ present an opportunity for improved performance at lower plasma current, though the underlying mechanisms which enable higher values of central safety factor are still under investigation ([5, 10–12] and references in [10]). Nonetheless, the successful development of such modes of operation may relax some of the operational constraints and also enable longer duration discharges, which are important for addressing various technology issues especially those dependent on neutron fluence such as the operation of the (tritium breeding) test blanket modules.

These sensitivity studies reinforced the importance of reliably operating ITER at full toroidal field, plasma current and elongation for the baseline scenario to fulfill its scientific and technology mission and underlined the impact of design or operational decisions, which could reduce the energy confinement time.

3. Poloidal field coil requirements

The unique combination of high current, high fusion power and long pulse operation in ITER results in very stringent demands on the poloidal field system to provide adequate flux swing, to control the plasma shape, including vertical position, the location of the divertor strike points and the distance to the first wall, in the presence of disturbances. These are often inter-related issues affecting the design requirements for the poloidal field system, since all poloidal field and central solenoid coils shown in figure 3 participate in providing plasma position, shape and current control.

Analysis of the plasma shape control has, to date, focused on the requirements to develop satisfactory current ramp-up and burn phases of the 15 MA reference scenario, while exploration of possible scenarios for the current ramp-down phase is continuing [13]. This analysis has benefited from additional experimental results [14–16]. The variation of the internal inductance during the different phases of the discharge is shown in figure 4 for a set of 'ITER demonstration

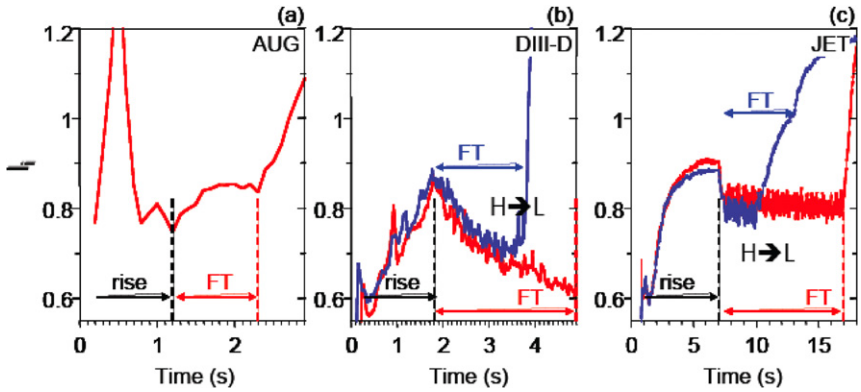

Figure 4. The l_i evolution for ITER demonstration discharges at $q_{95} = 3$. All discharges enter H-mode at the start of the flat-top. On the left (*a*) data from AUG, in the middle, (*b*) data from DIII-D and on the right, (*c*) data from JET. The red curves for DIII-D and JET with the longest flat-top phase available. The discharges indicated in blue have a deliberate step down of the heating power at 3.5 s for DIII-D and at 10 s for JET to provoke a transition back to L-mode (from [14]).

discharges', which were performed on JET, ASDEX-U and DIII-D, to simulate the evolution of the $Q = 10$ scenario [14]. These experiments have provided valuable input to both the design of the poloidal field system and requirements for the vertical stabilization (VS) system. A large aperture startup has replaced the variable aperture startup, originally envisioned for ITER, and when combined with an early transition to a divertor configuration and plasma heating, produces a plasma which is more vertically stable, reduces heat loads to the first wall and prevents excessive flux consumption prior to the start of the burn phase. The experimental results have indicated that the rapid development of a high edge pedestal leads to a rapid decrease in $l_i(3)$ after the onset of the H-mode and a slower decline to values as low as 0.6 towards the end-of-burn, somewhat outside the original reference range of $0.7 \leqslant l_i(3) \leqslant 1.0$ specified for the original design of the ITER poloidal field control system. Note that $l_i(3)$ is defined by

$$l_i(3) = \frac{2V\langle B_p^2\rangle}{(\mu_0 I)^2 R}. \quad (1)$$

The ITER 15 MA reference scenario has been analysed with several time-dependent and equilibrium codes [13]. To enable operation of low inductance discharges characteristic of H-mode operation, the design has been modified to: upgrade the current and field capability of the poloidal field conductor (recent R&D results confirm that the PF conductor performance is better than originally specified [3]); increase the number of turns in PF2 and PF6; increase the limit on the central solenoid vertical separation forces (from 75 to 120 MN), based on a detailed stress analysis of the central solenoid; relocate PF6 towards the plasma by 9 cm and radially by 7 cm; sub-cool the PF set to about 3.8 K; and modify the divertor slots and dome geometry, reducing the dome height by ~9 cm and shifting the target plate, as shown in figure 5. Current analysis is focusing on analysing the effect of plasma disturbances on the operating range and a detailed assessment of ramp-down phase of the discharge including the H to L transition.

Figure 6 illustrates the impact of the changes to the design of poloidal field system to enable access to low inductance discharges, characteristic of high performance H-mode operation. For reference, ~30 V s is required to

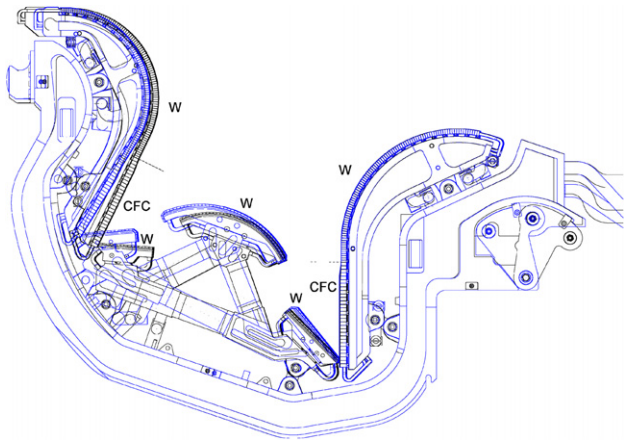

Figure 5. Proposed changes to the divertor dome and target plate locations to improve the location of the strike points in low inductance discharges. The new locations are shown in black.

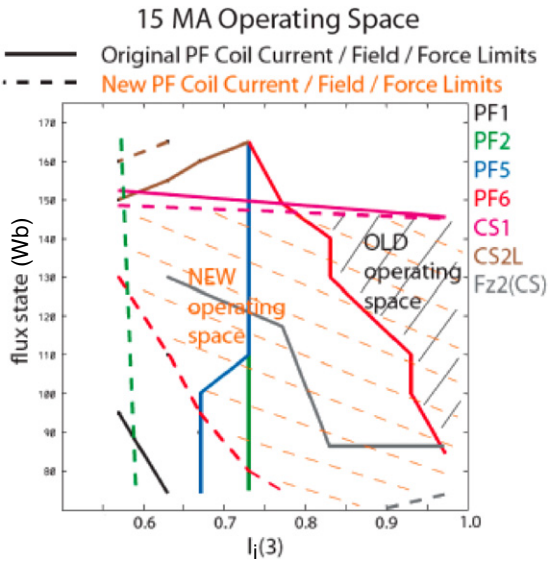

Figure 6. Available operational space at SOB in terms of flux state versus $l_i(3)$, with boundaries delimited by various coil limits (from [13]).

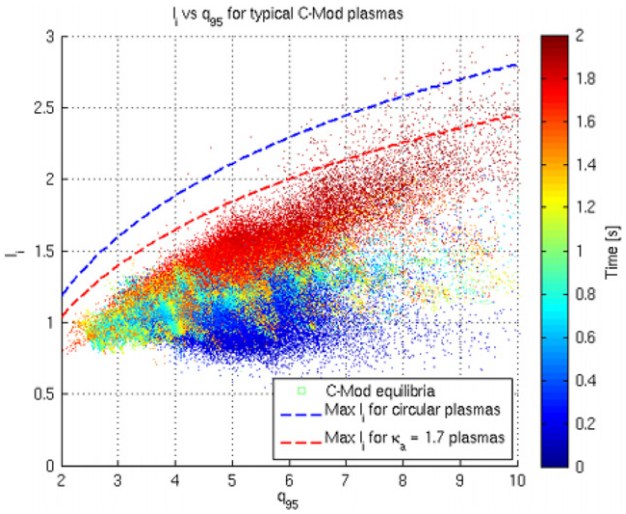

Figure 7. Database of the variation in $l_i(3)$ in C-Mod discharges. For comparison, the ITER operating range for vertical stability control of the original coil design is illustrated (from [17]).

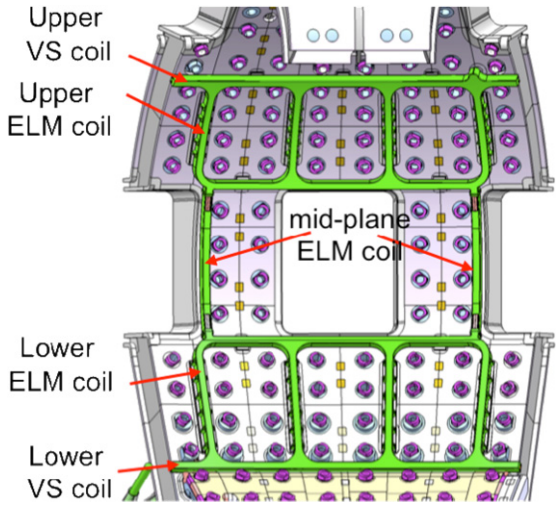

Figure 8. Proposed design of in-vessel coils for VS and ELM control. The ELM control windings can also be used for resistive wall stabilization.

sustain a 400 s burn phase. Thus, between the upper curves, set by the constraints on CS1 coil at end-of-burn, and lower curves, set typically by PF6 at start-of-burn (SOB), a gap of ~30 V s is required. This calculation for the PF6 limit from [13] is confirmed by several other analysis codes. Accepting greater deformation of the plasma boundary will enable access to increased operating space; however, accommodating the control response requirements associated with plasma disturbances will decrease operating space [13].

Current analysis is focusing on completing the review of the shape control capability for the reference scenario and refining the physics specification by

(i) detailing the impact of plasma disturbances on the operating range;
(ii) detailed assessment of ramp-down phase of the discharge including the H to L transition;
(iii) simulation of actual heating and current drive sources in ramp-up showing the associated volt-seconds savings and current profile evolution; and
(iv) completion of 17 MA scenario assessment

4. Vertical stability

Loss of vertical plasma position control in ITER will cause large thermal loads on plasma-facing components and also generate the highest electromagnetic loads. Performance of the ITER VS system has been analysed taking into account results from present devices. These results show, in particular, that in the current ramp-up and flat-top of the 15 MA, $Q = 10$ reference scenario, a range of internal inductance, $0.6 \leqslant l_i(3) \leqslant 1.2$, is likely to occur, as shown in figure 7 from C-Mod [17]. In the current decay, $l_i(3)$ can rise to even higher values and in this phase scenario adjustments (e.g. reducing elongation) will be required to maintain acceptable vertical stability. Studies are continuing on the current ramp-down phase for the reference $Q = 10$ scenario.

The parameter, $\Delta Z_{max}/a$, has been identified as a figure of merit for characterizing the effectiveness of the VS, where ΔZ_{max} is the maximum 'sudden' plasma displacement, which can be stabilized. Thus, the larger the value of $\Delta Z_{max}/a$, the greater the vertical control capability and robustness. In present devices, $\Delta Z_{max}/a > 0.05$ is required for reliable VS with robust stability achieved with $\Delta Z_{max}/a > 0.1$ [18, 19].

To provide reliable operation at the elongation required, an in-vessel coil system, shown in figure 8, has been proposed for increased vertical stability, the application of resonant magnetic perturbations (RMPs) to stabilize ELMs, and feedback stabilization of resistive wall modes (RWMs). Analysis performed to date indicates that this system will satisfy the requirement that values of $\Delta Z_{max}/a$ of at least 0.05 can be stabilized at acceptable levels of current and voltage and that it can control the plasma vertical position with minimal overshoot—on-going design analysis is aiming to achieve values of $\Delta Z_{max}/a$ of up to 0.10 over as large a range of parameters as possible. For comparison, the VS system was originally only able to achieve $\Delta Z_{max}/a$ of ~0.02 [13]. Studies of the performance of the VS system are continuing to set the specification of the voltage and current requirements of the internal coil system. The analysis to date indicates that these coils will adequately address the VS requirements.

5. Effect of toroidal field ripple on thermal confinement

Toroidal field ripple, which is defined as $(B_{max} - B_{min})/(B_{max} + B_{min})$, where B_{max} and B_{min} are the maximum and the minimum values of the toroidal magnetic field calculated at the nominal radius of the plasma separatrix and at the low-field side equatorial plane, can affect the confinement of energetic particles (alpha particles and beam ions) and result in local heat deposition on plasma-facing components. Recent results from JT-60U [20] and JET [21] have shown that in H-mode toroidal field ripple can also affect the confinement of the thermal plasma.

The JT-60U experiments demonstrated that following the installation of ferritic inserts the energy confinement time is improved, as shown in figure 9, as the toroidal field ripple is

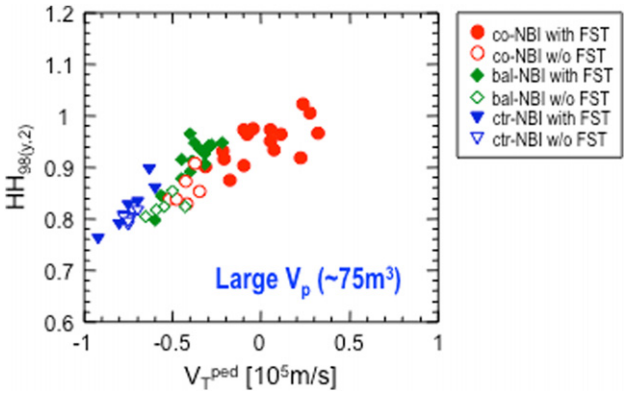

Figure 9. In the large bore JT-60U plasmas, the energy confinement factor increased with the installation of ferritic inserts (from [20]).

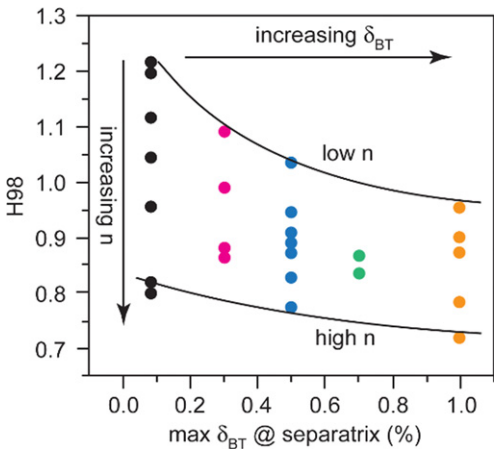

Figure 10. JET toroidal field ripple showing the variation of confinement time. At high density, the impact is modest; however in the low density, low collisionality regime, a reduction in confinement of up to 20% is observed (from [21]).

reduced from ∼1.7% to ∼1% on the average at the separatrix on the outer mid-plane in large aperture plasmas, taking into account the non-uniformity of the inserts. The energy confinement time improved by ∼15% due to the ferritic inserts and this improvement was accompanied by increased pedestal temperature, and the occurrence of larger ELMs. In addition, the edge toroidal velocity, which was in counter-direction with co-injected neutral beams without ferritic inserts, was observed to be in the co-direction when the ferritic inserts were installed (see figure 9). The JET experiments, by varying the currents in alternate toroidal field coils, were able to explore the impact of operating with lower ripple (0.08–1%) than the JT-60U experiments. These experiments also showed degradation in the energy confinement, pedestal height and plasma rotation with increasing TF ripple. The effect of ripple is strongest in the lower plasma density conditions as shown in figure 10. The JET experiments indicate that the decrease in H-mode confinement is continuous with ripple amplitude, although not necessarily linear. The deleterious effects of ripple are already visible at 0.3%, which corresponded to the first non-zero step in the JET ripple scans.

The experimental results indicate that the existing toroidal field ripple with the originally planned ferritic inserts may reduce the projected ITER performance. A study to reduce the ripple specification to 'as low as reasonably achievable' was approved. The underlying physics of how ripple affects plasma confinement, MHD stability and ELM behaviour is still an active area of research, as will be discussed further in the section on ELM control, where the proposed use of RMPs to control ELMs is reviewed. In addition to the toroidal field ripple, the (tritium breeding) test blanket modules will introduce field perturbations due to the ferromagnetic steel used in their structure. An acceptable level of perturbations or compensation techniques for the effects associated with the test blanket modules remains to be determined.

6. Plasma-facing materials in ITER

In addition to the constraints from heat load requirements, the selection of plasma-facing materials in ITER is based on a compromise amongst a series of physics and operational requirements, namely (a) minimum effect of impurity contamination on plasma performance and operation, (b) maximum operational flexibility at the start of operation and (c) minimum fuel retention for operation in the DT phase. This compromise is met by a choice of three plasma-facing materials at the beginning of operations (Be, C and W). It is planned to reduce the choices to two (Be and W) before DT operations in order to avoid long-term tritium retention in carbon co-deposits during the burning plasma phase.

Beryllium has been chosen for the first wall plasma-facing components to minimize fuel dilution caused by impurities released from these surfaces, which are expected to have the largest contamination efficiency [22–26] and the consequences of beryllium contamination on fusion performance and plasma operations are relatively mild. The small effect of beryllium on the core plasma has been extensively documented by experiments at JET at the highest currents and additional heating powers in both limiter and divertor configurations under conditions in which melting of the Be plasma-facing components was avoided (see [27] and references therein). On field lines intersecting the first wall, steady-state parallel particle and power fluxes during diverted operation in ITER are expected to be relatively low (<tens of MW m^{-2}) along the magnetic field lines, i.e. more than one order of magnitude lower than those at the separatrix. These low power flux values correspond to those of Ohmic limiter plasmas in JET, for which the improvement when using Be, in terms of plasma contamination and operational space with respect to carbon, were largest [28]. The main issues related to the use of Be in ITER are (a) the possible surface damage (melting) during transients such as ELMs and disruptions and its implications for operations and (b) the co-deposition of tritium with Be ([29, 30] and references in [29]) which is eroded from the first wall and deposited at the divertor targets (and possibly also locally redeposited into shadowed areas of the shaped ITER first wall). Both issues are part of on-going research, the initial results of which are being taken into account into the ITER design so that the influence of these two factors on ITER operation and mission are minimized (namely, ELM control systems based on pellets and RMP coils, disruption mitigation systems and increased temperature baking of the divertor to release tritium from Be-co-deposits).

Carbon is selected for the high power flux area of the divertor strike points for its compatibility with operation over a large range of plasma conditions and the absence of melting under transient loads. Both of these characteristics are considered to be essential during the initial phase of ITER exploitation in which plasma operational scenarios will require development and transient load control and mitigation systems will need to be demonstrated. Carbon divertor operation is expected to significantly ease the development of ramp-up scenarios for ITER, which are presently based on diverted low density plasmas with additional heating to a level of 20 MW [13]. In addition, the development of ELM mitigation strategies in the initial phases of operation (7.5 MA/2.65 T H-modes) will be considerably facilitated by the expectation that carbon impurity influxes during the worst uncontrolled ELMs under these conditions ($\Delta W_{\mathrm{ELM}} = 5$ MJ) are unlikely to cause plasma radiative collapses, which would probably trigger disruptions. Carbon also presents significant advantages for the development of disruption mitigation schemes since vapour shielding effects limit the erosion of the divertor target under the disruption power loads expected during the low activation phases of ITER to $<7\,\mu$m [31, 32]. Lack of melting ensures the absence of runaway growth of material damage or melt layer displacement [33] associated with W under high energy loads. The possible complications for plasma operation with surface-deformed components under the high power fluxes ($\sim$5–10 MW m^{-2}) expected at the separatrix are also avoided by using carbon.

The main open issue with this material choice concerns the consequences for long-term tritium retention in ITER associated with the deposition of hydrocarbon layers on hidden areas of the first wall during the initial operational phase. While this is still the subject of on-going R&D ([29, 34] and references in both), contributions from the EU Plasma–Wall Interaction task force and US Burning Plasma Organization have led to valuable insight [35, 36]. At present, operation with DT plasmas and carbon at the divertor strike zones is not foreseen in ITER because of the expected long-term in-vessel tritium retention associated with carbon erosion and hydrocarbon deposition and the lack of a removal method for such deposits that can be routinely applied in ITER. It is therefore planned to install a full tungsten divertor in advance of tritium operation since long-term tritium retention is predicted to be much lower than with carbon-based plasma-facing components [37]. By this stage of ITER exploitation, scenario development and steady-state and transient power flux control and mitigation schemes should be sufficiently developed that the probability of tungsten adversely affecting ITER operation and plasma performance is expected to be lower.

Tungsten has been chosen for the low power flux area of the divertor (baffles and divertor dome in the private flux region area) in order to limit the carbon source in the initial phase of operations. Given the low plasma fluxes expected in this area, simulations show that plasma contamination due to W originating from the baffles will be negligible [38] and its impact on plasma operation therefore very low. The compatibility of tungsten in this location with ICRF operation is the subject of on-going investigation in ASDEX Upgrade [26, 39] and in C-Mod [40, 41] using molybdenum. The installation of the ITER-like-wall in JET, a combination of beryllium and tungsten, will enable the evaluation of tungsten at even higher powers [42].

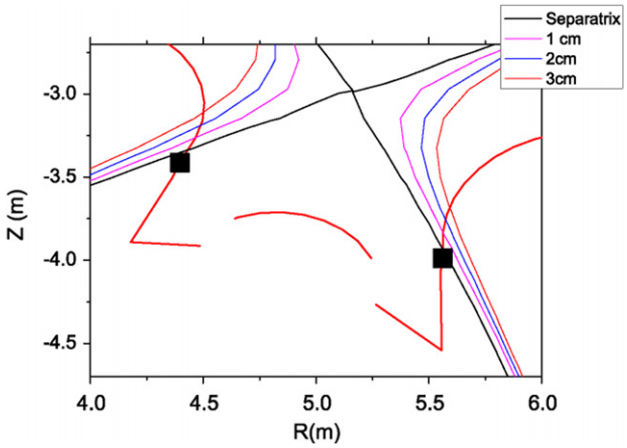

Figure 11. 7.5 MA H-mode plasma equilibrium in ITER with strike points on W baffle (CFC/W interface marked by black squares).

One of the drawbacks of the originally proposed ITER plasma-facing material strategy and divertor design described above was the delay in gaining operational experience with W as divertor target material at the strike zone in preparation for the tritium phase. In order to address this issue directly in ITER, its divertor design in ITER has been modified by increasing the extent of W onto the upper part of the vertical target (see figure 5). This enables operation at plasma currents of at least 7.5 MA on a vertical divertor W target (within PF coil and vertical stability limits), as shown in figure 11, all the while avoiding melting of W by transient loads during plasmas in which the strike zones are located on the carbon. The new ITER divertor design will thus allow earlier studies of the compatibility of ITER plasmas with a W divertor (development of scenarios, ELM control, operation on surface-damaged components by transient loads, etc) but still permits the development of discharges up to full plasma current (15 MA) on a more forgiving carbon target.

7. Heat load requirements for plasma-facing components

Results from present divertor tokamaks have shown that plasma fluxes to the main wall are dominated by intermittent events leading to fast plasma particle transport, which reaches the plasma-facing components along the magnetic field ([29] and references therein). The quasi-stationary heat fluxes to the main wall are thought to be dominated by convective transport [29, 34]. Although the steady-state parallel power fluxes associated with these particle fluxes will only be of the order of several MW m^{-2} in the ITER $Q_{\mathrm{DT}} = 10$ reference scenario, local overheating of exposed edges of main wall plasma-facing components can occur due to limitations in the achievable alignment tolerances. Similarly, transient events are expected to cause significant power fluxes to reach first wall panels in ITER along the field line. The expected loads from ELMs in ITER cover the range of parallel energy fluxes reaching the beryllium first wall from 1.0 MJ m^{-2} (controlled ELMs) to 20 MJ m^{-2} (uncontrolled ELMs) [43]. Even for

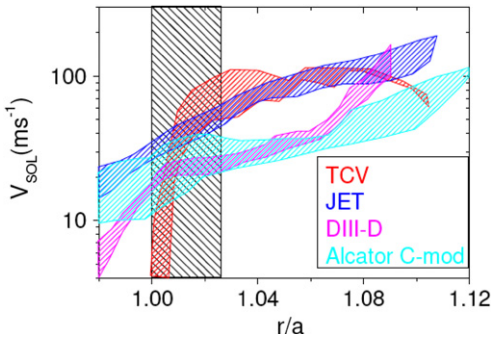

Figure 12. Derived effective plasma velocity in the SOL of various divertor tokamaks versus normalized distance to the separatrix. The near SOL to far SOL division in this figure coincides with 'standard' ITER operation near double null with a distance between the two separatrices $\Delta R_{sep} = 0.05$ m (from [43], based on data from [45–47]).

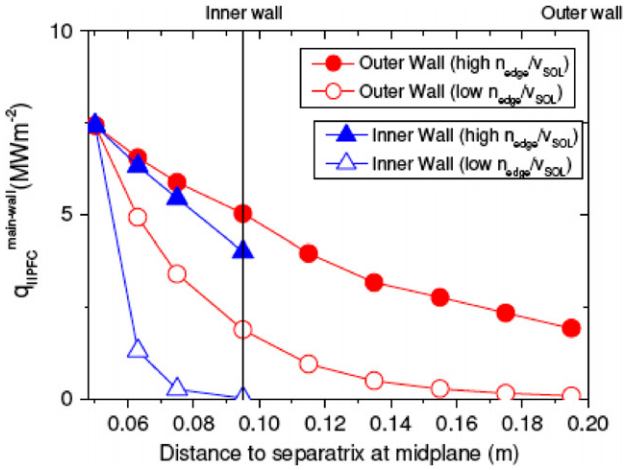

Figure 13. Calculated parallel power flux on the inner and outer wall for a range of assumptions concerning far-SOL transport for the ITER $Q_{DT} = 10$ scenario (from [43].

controlled ELMs, such energy fluxes are likely to cause melting of up to several tens of micrometres of beryllium at the exposed edges [44], which could cause undesirable impurity influxes at every ELM.

The ITPA divertor and SOL, MHD and pedestal groups provided key and timely data for this assessment [29, 34], in addition to the contributions from the EU Plasma–Wall Interaction task force and US Burning Plasma Organization. A multi-machine database in conjunction with modelling was used to extrapolate to ITER. This enabled an assessment of the thermal loads to the first wall and divertor, the specification for loads for all phases of discharge, a revision of specifications for vertical displacement events (VDEs), physics-based specifications for divertor re-attachment events during the full performance phase and transient loads associated with ELMs. Loarte *et al* [43] provides a detailed discussion of the physics basis for the revised requirement. As an example of this analysis, the role of 'blob' transport in the edge region can be characterized by an effective radial velocity for particle transport ([43], based on data from [45–47]), as shown in figure 12. The effective velocity in the far scrape-off region is used to estimate the parallel heat fluxes shown in figure 13 and predicts that the maximum values of the fluxes are at the upper region of the device (near the second X-point). Lowry *et al* [48] describes how the design of the first wall components has changed by taking into consideration the parallel heat fluxes, effect of ELMs and halo currents during disruptions. In particular, the first wall of the blanket shield module is being contoured to reduce the heat load to the leading edges and the modules in the vicinity of the ports are recessed, as shown in figure 14.

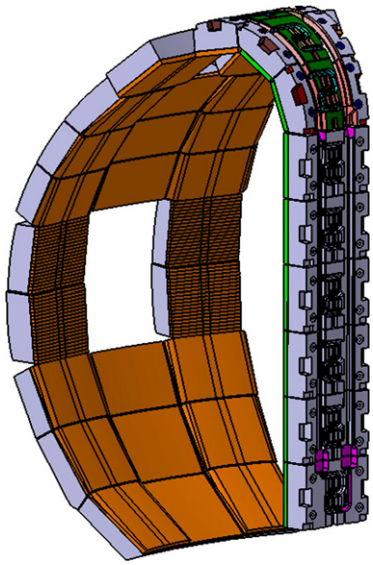

Figure 14. View of the low-field side first wall surface showing how the panels in line with the port openings are recessed with respect to those between (from [48]).

8. Edge localized modes (ELMs) control

ELMs can be driven by the large pressure gradients and current densities associated with the very small energy diffusivity of the H-mode plasma edge. Extrapolations from existing experiments to ITER indicate that unmitigated ELMs on ITER would correspond to $\Delta W_{ELM}/W_{ped}$ values of up to ~0.2 or ~20 MJ energy loss per ELM as indicated in figure 15 [49]. Oyama [50] notes that in recent JT-60U data even at low collisionalities the ELM amplitude varies substantially depending on among other parameters the plasma rotation and toroidal field ripple in the edge region. With counter-rotation in the edge, $\Delta W_{ELM}/W_{ped}$ values of 0.02–0.03 were achieved on JT-60U; in contrast, in JET experiments with low toroidal field ripple values $\Delta W_{ELM}/W_{ped}$ values of 0.25 were achieved. The smaller ELMs on JT-60U with counter rotation were accompanied by reduced confinement as shown in figure 9. A broader discussion of regimes of operation with small ELMs (e.g. Type II, Grassy or Type V) as well as alternate operating regimes such as QH or EDA modes, which do not have Type 1 ELMs but have another instability in the edge which avoids impurity accumulation, can be found in [5, 50].

Recent analyses by the ITPA of divertor heat loads due to ELMs indicate that the peak heat loads are projected to be greater since the heat fluxes are more localized relative to the analysis in the Progress in the ITER Physics Basis [29]. In addition, new information about material damage for both carbon fibre composite and tungsten divertor targets

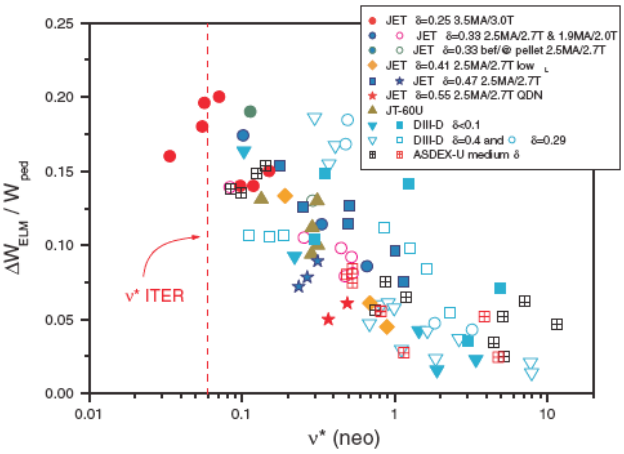

Figure 15. The pedestal stored energy in ITER for the baseline high performance H-mode scenario is ∼100 MJ, implying that the energy loss per ELM can be ∼20 MJ at the collisionalities expected in ITER edge (from [49]).

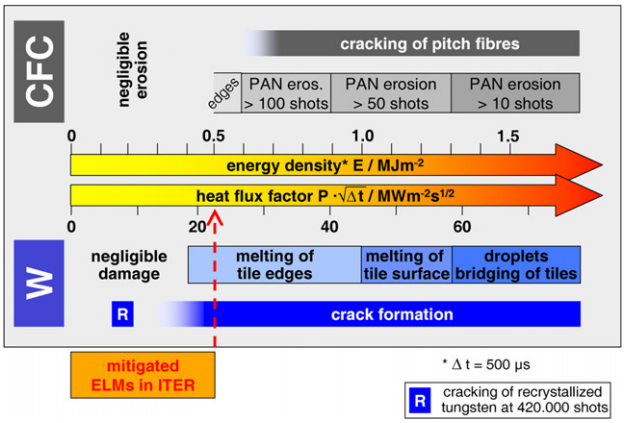

Figure 16. Overview of damage to carbon fibre composite and tungsten divertor targets by ELMs. This analysis indicates that the transient heat load from ELMs needs to be reduced to about 0.5 MJ m^{-2}. For comparison, unmitigated ELMs correspond to ∼10 MJ m^{-2} (from [51] and references therein).

has become available as shown in figure 16 [51, 52]. The conclusion is that an incident energy impulse of more than ∼0.3% of the total thermal plasma energy (∼1 MJ) can cause tile fatigue and cracking as well as erosion, and larger energy losses can ablate or melt divertor materials, potentially degrading the purity of ITER plasmas and greatly reducing the lifetime of the ITER divertor. These results imply a need to reduce the energy impulse by a factor of ∼20 and being able to do so very reliably. For 1000 high power shots, the 20 MJ ELMs would have to be reduced to ∼10^7 1 MJ ELMs, corresponding to 0.5 MJ m^{-2}. Occasional ELMs beyond the 0.5 MJ m^{-2} are acceptable if limited to ∼1.0–1.5 MJ m^{-2} (CFC) and ∼1.0 MJ m^{-2} (W melting occurs). The consequences of thermal fatigue of 10^7 1 MJ ELMs remains to be established since cracks are observed after material testing of both tungsten and CFC target materials [51].

Tools that can either eliminate or greatly reduce ELM energy losses without significantly degrading confinement are therefore critically important for successful operation of ITER and have stimulated further worldwide research on

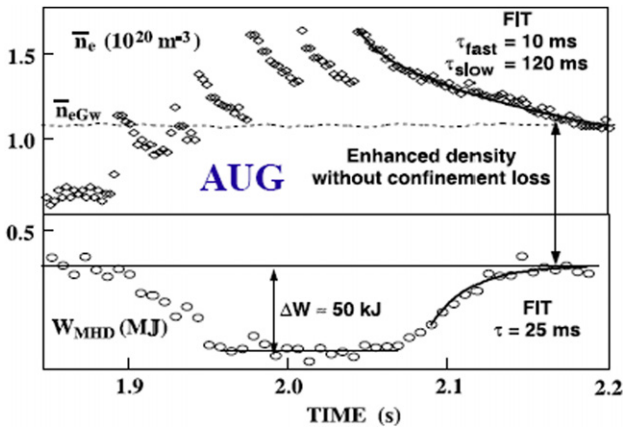

Figure 17. Impact of pellet injection in ASDEX Upgrade on confinement time, showing a modest degradation in the energy confinement, which is attributed to convective energy loss (from [73]).

ELMs [5, 29, 31, 53–68]. Two approaches, pellet pacing and application of helically RMPs, are current areas of experimental and theoretical research that were evaluated as part of the ITER Design Review [68]. In addition, vertical position 'joggling', first used to pace ELMs on TCV [69] and AUG [70], has recently been exploited on JET [71]. Though it is not clear what poloidal field power would be required to do this in ITER, nor indeed if it would work at all, the JET 'vertical joggling' experiments show that ELMs can be paced to a frequency at least an order of magnitude greater than the 'natural' frequency. This result is encouraging not only for this technique but also related approaches such as pellet pacing used to stimulate smaller ELMs. However, as will be discussed further below, it is not evident that the continued inverse proportional reduction of ELM energy loss with frequency can be depended upon and further research is required.

Experiments on ASDEX Upgrade, DIII-D and JET have demonstrated that pellets can trigger ELMs, enabling the production of more frequent smaller ELMs. The energy loss per ELM event was reduced by 40% by the application of pellet pacing to control the ELM frequency though even larger reductions have been observed in uncontrolled experiments in which the pellet was injected right after a naturally occurring ELM [72]. The experiments are accompanied by a small degradation in the energy confinement time, which is associated with increased convective loss as shown in figure 17 [73]. Pellet pacing to control ELMs on ITER is a significant extrapolation from current experiments because the ratio of the pellet repetition time to the energy confinement time is much smaller.

The frequency of pellet injection required on ITER to reduce the ELM energy loss to acceptable levels is estimated to be about 20–40 Hz with pellets penetrating to the top of the pedestal. Lang *et al* [72] showed that the energy confinement time scales as $f_{\mathrm{ELM}}^{-0.16}$, with relatively large pellets. If this scaling were applicable and the ELM frequency were increased by a factor of 20 to reduce the heat load to an acceptable level, the confinement time reduction when extrapolated to ITER of ∼40% would be unacceptable. It is also possible to estimate the convective energy loss taking into account that the particle

confinement time decreases with increasing minor radius as observed on MAST [74] and depth of pellet penetration using existing pellet technology. For these assumptions, the convective power loss is also estimated to be a significant fraction of the heating power. To decrease the adverse effects of the accompanying convective energy loss at this frequency and depth of penetration will require the development of a higher speed pellet injector [54] utilizing smaller pellets. Further experimental results are needed to refine the requirements for the depth of penetration required to trigger ELMs and evaluate the impact on energy confinement when using higher frequency pellet injectors.

To provide for the capability to incorporate pellet pacing on ITER, the gas throughput requirements were updated. The gas throughput requirements for 400 s standard burn pulses were increased from 120 to ~200 Pa m^3 s^{-1}. For 1000 s pulses the gas throughput was increased from 120 to 160 Pa m^3 s^{-1}. The requirement for 3000 s pulses were maintained at 120 Pa m^3 s^{-1}. The requirements for the pellet injector will be updated after further experimental results from existing machines become available.

The application of RMPs to control ELMs began with early work on JFT-2M [75] and is currently a very active area of research. Different experimental results have been obtained, depending on the applied perturbation mode spectrum ([53, 56, 62–64, 66, 71] and references in [53]). These include (1) triggering ELMs in a previously ELM-free discharge (COMPASS, JFT-2M and NSTX) with $n = 3$ fields from large aperture, external (far from the plasma) RMP coils on the outer mid-plane, (2) increasing the frequency of ELMs and reducing the amplitude on DIII-D and JET using $n = 1$ or $n = 2$ perturbations from both large aperture, external, mid-plane coils and smaller aperture, internal off-mid-plane rows of coils, to (3) fully suppressing ELMs on DIII-D with $n = 3$ RMPs from small aperture, internal, off-mid-plane rows of coils. The ability to completely suppress Type I ELMs has major implications for the reliability of plasma-facing components and has motivated the inclusion of a capability to apply RMPs into the ITER design.

The use of RMPs for ELM control to suppress ELMs on DIII-D involves applying helically RMPs to the plasma boundary to increase the plasma transport near the edge and thereby limit the edge pressure gradient of the H-mode. This technique has been shown to be capable of suppressing ELMs at ITER-relevant collisionality while maintaining the energy confinement times consistent with the predictions of the ITER database ($H_{98y,2} = 1$) provided the magnetic perturbations are sufficiently localized to the plasma edge region.

The DIII-D data, in combination with the results from the other devices, provide four guidelines toward the requirements for ELM suppression coils on ITER: (1) the coils should be as close as possible to the plasma to maximize the edge perturbation while minimizing the core perturbation, (2) the coil rows should be on the outboard side but not solely on the outboard mid-plane, (3) the perturbation should be as pitch aligned with the unperturbed equilibrium field lines as possible and (4) the width of the edge region having good overlap of magnetic islands calculated with the vacuum fields from the coils should be greater than a threshold value. Overlap of magnetic islands and significant field-line stochasticity can

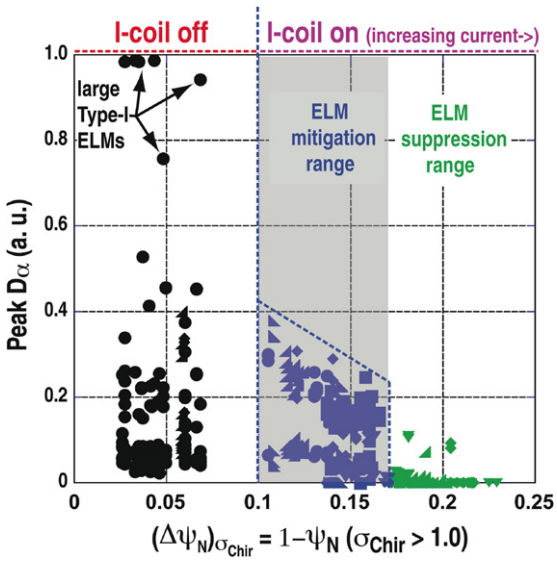

Figure 18. Results from DIII-D experiments at $q_{95} \sim 3.6$ for the ITER shape and edge collisionality. The maximum ELM size is correlated with the width of the edge region having Chirikov overlap parameter greater than 1.0 and ELM suppression is correlated with the overlap width exceeding a threshold value (from [53]).

be characterized by a Chirikov parameter (magnetic island width/island spacing) being greater than 1.0. In the DIII-D analysis [53], the Chirikov parameter is based on vacuum calculations of RMP mode components excluding the plasma response or rotational shielding. The maximum ELM size in the DIII-D experiments at $q_{95} \sim 3.6$ is correlated with the width of the edge region having Chirikov parameter >1 (figure 18). The results shown in figure 18 rely on D_α measurements and these trends have been confirmed by fast magnetic measurements. The threshold value for the ELM suppression range from these experiments was used to guide the requirements for the currents in the ITER coil design.

With the existing geometry of the internal plus external coils on DIII-D, the requirement for field line alignment results in suppression being achieved in a relatively narrow range of the safety factor, $3.2 < q_{95} < 3.8$, when the two rows of internal coils are configured with up–down symmetric perturbations, in combination with $n = 1$ fields from the external coil, which are typically used to correct error fields. For up–down asymmetric perturbations from the internal coils, field line alignment and ELM suppression occur again at $q_{95} \sim 7.2$, confirming the requirement for pitch alignment of the perturbation fields. Outside these pitch aligned resonant windows in q_{95}, ELM energy loss is reduced when the perturbations are applied, but ELMs are not suppressed. The DIII-D experiments utilized two rows of off mid-plane coils to create an $n = 3$ helical pattern. In contrast, other experiments, including experiments on DIII-D, which utilized one row of distant mid-plane coils did not succeed in suppressing ELMs before generating locked modes. On MAST and NSTX, experiments using their outboard mid-plane error field correction coils also failed to suppress ELMs, though the Chirikov parameter was estimated to satisfy the criteria developed from the experiments with good pitch aligned RMPs from the internal coils on DIII-D. However, in DIII-D a single row of off mid-plane in-vessel coils did suppress ELMs before

locking, perhaps because the coil set close to the plasma has less non-resonant spectral content relative to resonant than fields from more distant coils. These results suggest the importance of the mode spectrum.

A comprehensive understanding of the underlying physics is still emerging, motivating additional experiments, including the role of edge pumping and pellet injection. Variation of the location of the strikepoint with respect to the DIII-D cryopanels demonstrated that edge pumping is an important consideration. Furthermore, the effective particle confinement time decreased in DIII-D experiments, with the application of RMP coils decreasing the plasma density, but that should, in principle, be able to be compensated with increased core pellet fuelling. The complex relationship between the conditions in the pedestal, which are affected by the RMP coils, and the core confinement is still under investigation. Pellet injection into discharges with RMPs has in some cases, but not always, triggered ELMs. Since pellet fuelling is integral to achieving the required densities in ITER, this needs to be studied further. This has also motivated further theoretical work on the role of resonant and non-RMPs, which is important not only for ELM suppression but, more broadly, for error field correction and avoidance of locked modes [55, 76]. A closely related issue that needs to be more thoroughly explored is not only the impact of the magnetic perturbations on plasma rotation but the role of plasma rotation in the penetration of the magnetic field perturbation and changes in transport in the edge pedestal [55, 76–78].

In support of the ITER in-vessel coil design, experimental and theoretical assessments were performed for different coil configurations to evaluate the magnetic spectrum and the coil current requirements. As discussed above, this analysis indicates that multiple (3) rows of in-vessel coils provide greater flexibility to attain the minimum conditions for ELM suppression and minimize the deleterious effects of plasma rotation damping. As shown in figure 8, three rows of coils, with one row above, one row below and one row on the mid-plane, are proposed for each of the nine vessel sectors enabling an $n = 3$ mode spectrum and field line alignment. These coils would be located behind the blanket shield modules, and provisions are included to enable remote maintenance of the coils. Though there has been substantial progress in defining the physics and engineering requirements for the coil design, the criteria for field line alignment and mode spectrum, as well as magnitude of the perturbed field, remains an active area of research. ELM control and mitigation is important for the success of the ITER programmes and warrants the scientific attention that is being given to it.

9. Resistive wall modes

An important goal of ITER is to demonstrate steady-state-compatible operation at moderate fusion gain ($Q = 5$). Operation in 'steady-state' regimes in ITER, such as the reference scenario 4, entails operation at high normalized pressure ($\beta_N > 3$), which can destabilize a RWM ([79] and references therein). Even if plasma conditions allow for RWM stabilization for a given plasma rotation profile and magnitude, the damping will be weak, allowing the RWM to be easily excited to finite amplitude by static error fields [80] or by other

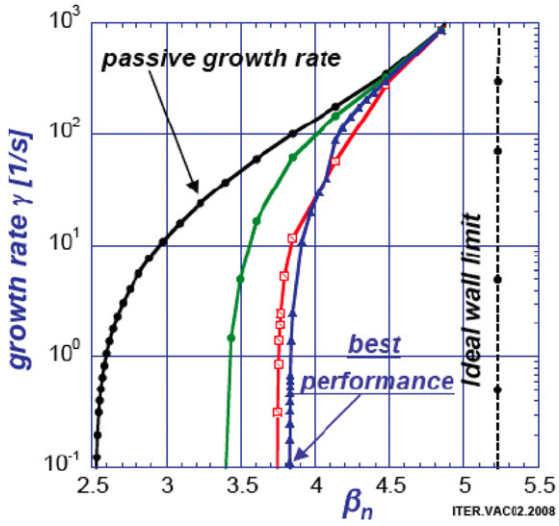

Figure 19. VALEN calculations of the growth rate showing ability to control the RWM. The green curve corresponds to using only the mid-plane coils, the blue corresponds to using the upper and lower coils and the red corresponds to using all three sets of coils.

MHD events [81]. For this reason, active feedback control of the RWM is necessary in ITER. Experiments on DIII-D and NSTX have shown that feedback control of the unstable RWM at low rotation is possible provided the mode identification and control field response are sufficiently rapid [82].

In-vessel coils such as those shown in figure 8 can also be used to generate an n=1 field for RWM control. As shown in figure 19, the VALEN-3D code [83] for a plasma with a predicted no-wall limit on $\beta_N = 2.52$ with a single-mode model predicts superior performance when all three toroidal rows of coils are used (stabilized $\beta_N = 3.74$) compared with mid-plane coils (stabilized $\beta_N = 3.39$). The use of just the top and bottom coils is predicted to achieve very similar values of 3.83, which is equivalent to the performance of using all three poloidal rows of coils given the level of optimization performed in the calculations.

Improved performance with multiple toroidal coil arrays is expected due to superior mode coupling and phasing between the larger array of control coils and the mode. Although a complete, benchmarked physical model of multiple RWM mode effects is presently not available, on-going development of such codes and the underlying theory suggests that a single-mode model may be adequate for a stable RWM, while a strongly unstable RWM requires a multi-mode description including nearby stable modes [84]. Consequently, inferior spectra of the control field may help drive weakly stable modes to finite amplitude (mode non-rigidity), which may also interfere with mode detection of the unstable mode. Experimentally, mode non-rigidity has been observed on NSTX during $n = 1$ feedback [82]. Poloidal mode deformation that leads to either up/down asymmetry of the mode amplitude, or up/down symmetry with mid-plane bulging of the mode has been observed with a single mid-plane control coil and off-mid-plane sensors. Multiple rows of coils in ITER will allow the spectrum of the applied field to be best matched to the unstable mode, reducing the relative amplitude of the undesired sidebands and if necessary stabilize $n = 2$ or

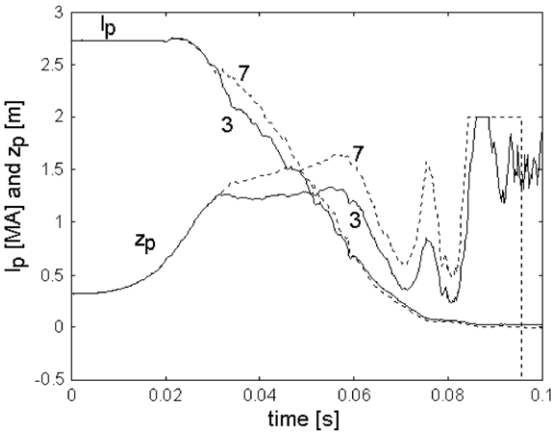

Figure 20. Plasma current and vertical position, in the opposite octants 3 and 7, during a deliberately provoked VDE in JET (from [89]).

$n = 3$ modes. Analysis of the coil current requirements for RWM control [82, 85] is ongoing.

10. Disruptions and disruption mitigation

ITER will have the largest plasma current, and therefore stored plasma and magnetic energy, of any magnetic confinement facility. Hence, plasma disruptions will have the greatest potential impact on ITER due to runaway electron generation [86, 87] as well as from the release of the stored thermal and magnetic energy ([79, 88–100] and references in [79]). Recent application of JET data shown in figure 20 [89] to the ITER design has identified the need to take into account additional electromagnetic forces due to the presence of a non-rotating kink mode during a VDE. In addition to the vertical loads due to the VDE, which are the dominant loads, the kink mode results in a 'sideways' (horizontal) force on the vessel. The force scaling has been determined in [88] and used for assessment of forces on the ITER vessel. Based on JET data [89], the 'sink–source' model was used for the sideway forces that can be attributed to the current sharing between plasma and the vessel. The recent theory [90] described a new, 'wall touching kink mode' and explained the mechanism of the current sharing by excitation of the surface currents excited by the kink mode. This theory predicts the same global forces. Unlike the vertical forces and halo currents, which have been extensively studied on a number of machines, the sideways force has been documented on JET, but not observed to be as large on other machines ([79] and references therein). Further experimental results and theoretical analysis would be valuable to improve the extrapolation of forces and tilting moments to ITER. The vacuum vessel load requirements, taking into account a factor of 1.2 for differences between DINA modelling and results on JT-60U, were revised from a peak horizontal force of 25–50 MN, while the peak downward vertical force was revised from 75 to 108 MN, and a requirement for the tilting moment of ~215 MN m was incorporated. The most critical area of the vacuum vessel affected by the increased electromagnetic loads on the vacuum vessel structure is the connection of the lower port to the main vacuum vessel shell. To accommodate the change in the design loads, the poloidal gussets supporting the vessel have been reinforced as shown in figure 21.

To ameliorate the impact of a disruption on ITER operations, massive gas injection is proposed to radiatively terminate the plasma discharge, which alleviates plasma power loading on plasma-facing materials and minimizes halo currents ([79] and references therein). However in ITER, mostly due to its large plasma current, a further requirement is that runaway electrons be suppressed. A large runaway electron current, >5 MA, is predicted to damage the beryllium tiles on the blanket shield modules when the runaway electron current is deposited on the first wall.

Although the details of the runaway confinement are not fully understood, the conservative approach to suppressing runaway electrons is to increase the collisional damping such that the density exceeds the commonly referred to 'Connor–Hastie' [86] or 'Rosenbluth' density [87] by the injection of large amounts of gas into the plasma volume prior to the current quench. The gas load requirements for helium have been estimated for ITER, assuming a fuelling efficiency of 20%, at up to 500 kPa m^3 [99]. There are significant engineering and operational implications associated with such a large gas load, as discussed by Whyte *et al* [99] and Pautasso *et al* [100]. The recent ASDEX-U experiments have achieved densities comparable to the 'Rosenbluth density' [100]. Experimental and theoretical work has shown that gas loads corresponding to the Connor–Hastie–Rosenbluth density are not needed in current experiments; however, current experiments may be operating in a different regime of runaway electron production due to the lower current. Further research on developing a more quantitative understanding of the gas loads, choice of gas or gas mixture, and the mechanism for introducing the particles into ITER for disruption mitigation and runaway suppression is needed, but ultimately this may only be resolved during the hydrogen commissioning phase of ITER.

Engineering studies indicate that pumping the torus down to the required operating pressure after the injection of ~500 kPa m^3 of gas appears possible in a time of 3–4 h with some additional optimization of the design, allowing an acceptable recovery time for plasma operation.

11. Summary

The results presented here were the result of an intense effort by the international community with major contributions by the ITPA. During this time, the core machine parameters were reaffirmed and many detailed issues were addressed to ensure that the ITER Project would meet its mission requirements. The poloidal field coil system was reviewed and modified to ensure that the plasma can be adequately controlled. Stabilization of the vertical disruption event was addressed by including in the design in-vessel coils. Recent results regarding the impact of toroidal field ripple were taken into account by modifying the ripple requirements. The impact of ELMs on plasma-facing components was recognized as an important issue, which, if not addressed, could have adverse impacts on the plasma-facing components. As a result, the requirements for gas loads in support of pellet pacing were increased and the in-vessel coils were designed to apply a RMP to control ELMs. The design of the vacuum vessel was changed as a result of recognizing the implications of

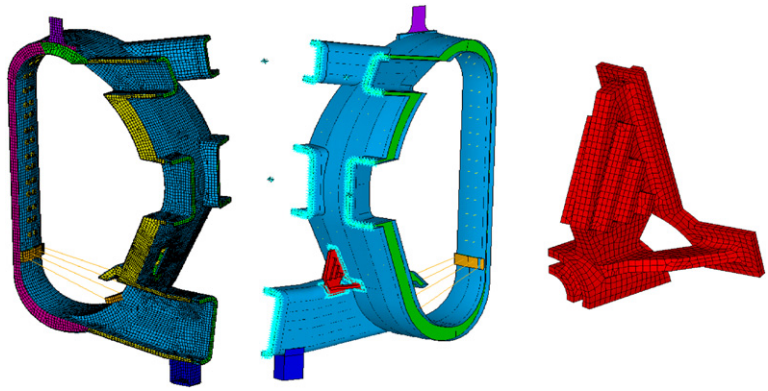

Figure 21. Reinforcement of the lower port connection to the main ITER vacuum vessel shell is shown in red. Only one of the two gussets is shown.

prior results on JET and associated modelling. The impact of runaway electron mitigation was assessed.

This work has motivated further research in these areas including extensive discussions and detailed planning for joint experiments within the ITPA, which will enable refinements of the design requirements and support planning for the operational phase. For example, the power threshold for H-mode operation has important ramifications for the hydrogen and deuterium phase of operation. Development of operational regimes in which ELMs are stabilized while avoiding impurity accumulation can have great benefit. Continued close interaction between the ITER Organization and the international scientific and technical community will be critical to ensure that optimal use is made of ITER. The ITER Organization, through its focus on the construction of the project, identifies important problems of interest to the scientific community. The scientific community, through its on-going research program, identifies solutions to problems that have not yet been articulated. This synergy is valuable and should be maintained beyond the design phase.

This report was prepared as an account of work by or for the ITER Organization. The Members of the Organization are the People's Republic of China, the European Atomic Energy Community, the Republic of India, Japan, the Republic of Korea, the Russian Federation and the United States of America. The views and opinions expressed herein do not necessarily reflect those of the Members or any agency thereof. Dissemination of the information in this paper is governed by the applicable terms of the ITER Joint Implementation Agreement. The work was supported in part by US DOE Contract DE-AC02-76CH03073.

References

Papers presented at the 22nd Int. Fusion Energy Conf. (Geneva) listed below can be found at http://www-naweb.iaea.org/napc/physics/FEC/FEC2008/html/index.htm

[1] Shimada M. *et al* 2007 Progress in the ITER Physics Basis *Nucl. Fusion* **47** S1
[2] Holtkamp N. *et al* 2008 The status of the ITER design *Proc. 22nd Int. Conf. on Fusion Energy 2008 (Geneva, Switzerland, 2008)* (Vienna: IAEA) OV/2-1
[3] Weng P. *et al* 2008 Results of ITER superconducting magnet R&D *Proc. 22nd Int. Conf. on Fusion Energy 2008 (Geneva, Switzerland, 2008)* (Vienna: IAEA) IT/1-3
[4] Alejaldre C. *et al* 2008 ITER on the way to become the first fusion nuclear installation *Proc. 22nd Int. Conf. on Fusion Energy 2008 (Geneva, Switzerland, 2008)* (Vienna: IAEA) IT/1-1
[5] Doyle E.J. *et al* 2007 Progress in the ITER Physics Basis *Nucl. Fusion* **47** S18
[6] Albajar F., Johner J. and Granata G. 2001 *Nucl. Fusion* **41** 665
[7] Martin Y.R. *et al* 2008 *J. Phys.: Conf. Ser.* **123** 012033
[8] Ryter F. *et al* 2008 H-mode threshold and confinement in helium, deuterium and hydrogen in ASDEX Upgrade *Proc. 22nd Int. Conf. on Fusion Energy 2008 (Geneva, Switzerland, 2008)* (Vienna: IAEA) PD/1-1
[9] Sartori R. *et al* 2002 *Plasma Phys. Control. Fusion* **44** 1801
[10] Gormezano C. *et al* 2007 Progress in the ITER Physics Basis *Nucl. Fusion* **47** S285
[11] Joffrin E.H. *et al* 2008 Development of the 'hybrid' scenario in JET *Proc. 22nd Int. Conf. on Fusion Energy 2008 (Geneva, Switzerland, 2008)* (Vienna: IAEA) EX/1-4Ra
[12] Petty C.C. *et al* 2008 Advances in the physics basis of the hybrid scenario on DIII-D *Proc. 22nd Int. Conf. on Fusion Energy 2008 (Geneva, Switzerland, 2008)* (Vienna: IAEA) EX/1-4b
[13] Kessel C.E. *et al* 2008 Development of ITER 15 MA ELMy H-mode inductive scenario *Proc. 22nd Int. Conf. on Fusion Energy 2008 (Geneva, Switzerland, 2008)* (Vienna: IAEA) IT/2-3
[14] Sips A.C.C. *et al* 2009 Experimental studies of ITER demonstration discharges *Nucl. Fusion* at press
[15] Jackson G.L. *et al* 2008 Simulating the ITER plasma startup scenario in the DIII-D tokamak *Proc. 22nd Int. Conf. on Fusion Energy 2008 (Geneva, Switzerland, 2008)* (Vienna: IAEA) IT/P7-2
[16] Luce T.C. *et al* 2008 *35th EPS Conf. on Plasma Physics (Hersonissos, Greece, 9–13 June 2008)* vol 32 (ECA) P-2.073
[17] Ferrara M., Hutchinson I.H. and Wolfe S.M. 2008 *Nucl. Fusion* **48** 065002
[18] Portone A. *et al* 2008 ITER plasma vertical stabilization *Proc. 22nd Int. Conf. on Fusion Energy 2008 (Geneva, Switzerland, 2008)* (Vienna: IAEA) IT/2-4Ra
[19] Humphreys D. A. *et al* 2008 Experimental vertical stability studies for ITER performance and design guidance *Proc. 22nd Int. Conf. on Fusion Energy 2008 (Geneva, Switzerland, 2008)* (Vienna: IAEA) IT/2-4Rb
[20] Urano H. *et al* 2007 *Nucl. Fusion* **47** 706
[21] Saibene F. *et al* 2008 Results of the variable toroidal field ripple experiments in JET *Proc. 22nd Int. Conf. on Fusion Energy 2008 (Geneva, Switzerland, 2008)* (Vienna: IAEA) EX/2-1
[22] McCracken G. *et al* 1997 *Phys. Plasmas* **4** 1681
[23] Lipschultz B. *et al* 2001 *Nucl. Fusion* **41** 585

[24] Strachan J. *et al* 2003 *Nucl. Fusion* **43** 922
[25] Kallenbach A. *et al* 2005 *Plasma Phys. Control. Fusion* **47** B207
[26] Dux R. *et al* 2009 Plasma–wall interaction and plasma behaviour in the non-boronised all tungsten ASDEX Upgrade *J. Nucl. Mater.* at press doi:10.1016/j.jnucmat.2009.01.225
[27] Loarte A. *et al* 2005 *J. Nucl. Mater.* **337–339** 816
[28] The JET Team: presented by P.R. Thomas 1991 *J. Nucl. Mater.* **176–177** 3
[29] Loarte A. *et al* 2007 Progress in the ITER Physics Basis *Nucl. Fusion* **47** S203
[30] Doerner R.P. *et al* 2009 Issues associated with codeposition of deuterium with ITER materials *Nucl. Fusion* **49** 035002
[31] Landman I.S. *et al* 2008 Integrated modelling of ITER plasma dynamics and wall processes following Type I ELMs and consequences for tokamak operation *Proc. 22nd Int. Conf. on Fusion Energy 2008 (Geneva, Switzerland, 2008)* (Vienna: IAEA) IT/P6-11
[32] Klimov N. *et al* 2009 Experimental study of PFCs erosion under ITER-like transient loads at plasma gun facility QSPA *J. Nucl. Mater.* at press doi:10.1016/j.jnucmat.2009.01.197
[33] Bazylev B *et al* 2008 Simulations of material damage to divertor and first Wall Armour under ITER transient loads by modelling and experiments *Proc. 22nd Int. Conf. on Fusion Energy 2008 (Geneva, Switzerland, 2008)* (Vienna: IAEA) IT/P6-10
[34] Lipschultz B. *et al* 2007 *Nucl. Fusion* **47** 1189
[35] Roth J. *et al* 2008 Recent analysis of key plasma wall interactions issues for ITER *Proc. 18th Int. Conf. on Plasma Surface Interactions 2008 (Toledo, Spain, 2008)* R-1 http://psi2008.ciemat.es/talks.shtml *J. Nucl. Mater.* submitted
[36] Brooks J.N. *et al* 2009 Plasma surface interaction issues of an all-metal ITER *Nucl. Fusion* **49** 035007
[37] Roth J. *et al* 2008 *Plasma Phys. Control. Fusion* **50** 103001
[38] Schmid K. *et al* 2007 *J. Nucl. Mater.* **363–365** 674
[39] Bobkov V. *et al* 2008 Operation of ICRF antennas in a full tungsten environment in ASDEX *Proc. 18th Int. Conf. on Plasma Surface Interactions 2008 (Toledo, Spain, 2008)* O-10 http://psi2008.ciemat.es/talks.shtml 2009 *J. Nucl. Mater.* doi:10.1016/j.jnucmat.2009.01.231 submitted
[40] Lipschultz B. *et al* 2006 *Phys. Plasmas* **13** 056117
[41] Wukitch S.J. *et al* ICRF specific impurity sources and plasma sheaths in Alcator C-Mod *J. Nucl. Mater.* at press doi:10.1016/j.jnucmat.2009.01.245
[42] Matthews G.F. *et al* 2007 *Phys. Scr.* **T128** 137–43
[43] Loarte A. *et al* 2008 Power and particle fluxes at the plasma edge of ITER: specifications and Physics Basis *Proc. 22nd Int. Conf. on Fusion Energy 2008 (Geneva, Switzerland, 2008)* (Vienna: IAEA) IT/P6-13
[44] Loarte A. *et al* 2005 *J. Nucl. Mater.* **337–339** 816
[45] Lipschultz B. *et al* 2003 A study of JET radial transport based on particle balance *Proc. 30th Eur. Conf. on Controlled Fusion and Plasma Physics (St Petersburg, Russia, 2003)* (Geneva: European Physical Society) http://epsppd.epfl.ch/StPetersburg/PDF/P3_197.PDF
[46] Lipschultz B. *et al* 2005 *Plasma Phys. Control. Fusion* **47** 1559
[47] Garcia O. *et al* 2007 *Nucl. Fusion* **47** 667
[48] Lowry C.G. *et al* 2008 Progress in design and R&D on ITER plasma facing components *Proc. 22nd Int. Conf. on Fusion Energy 2008 (Geneva, Switzerland, 2008)* (Vienna: IAEA) IT/1-4
[49] Loarte A. *et al* 2003 *Plasma Phys. Control. Fusion* **45** 1549
[50] Oyama N. 2008 *J. Phys.: Conf. Ser.* **123** 012002
[51] Linke J. *et al* 2008 *Proc. World Academy of Ceramics—FORUM 2008, Ceramic Materials in Energy Systems for Sustainable Development (Chianciano Terme, Italy, 5–8 July 2008)*
[52] Tereshin V.I. *et al* 2008 Simulation of ITER transient heat loads to the divertor surfaces with using the high power quasi-steady-state plasma accelerator *Proc. 22nd Int. Conf. on Fusion Energy 2008 (Geneva, Switzerland, 2008)* (Vienna: IAEA) IT/P6-12
[53] Fenstermacher M.E. *et al* 2008 *Phys. Plasmas* **15** 056122
[54] Baylor L.R. *et al* 2009 Pellet fueling, ELM pacing, and disruption mitigation technology development for ITER *Nucl. Fusion* at press
[55] Becoulet M. *et al* 2009 Physics of penetration of resonant magnetic perturbations used for Type I edge localized modes suppression in tokamaks *Nucl. Fusion* at press
[56] Evans T.E. *et al* 2008 Operating characteristics in DIII-D ELM-suppressed RMP H-modes with ITER similar shapes *Proc. 22nd Int. Conf. on Fusion Energy 2008 (Geneva, Switzerland, 2008)* (Vienna: IAEA) EX/4-1
[57] Fundamenski W. *et al* 2008 ELM filament heat loads on plasma facing components in JET and ITER *Proc. 22nd Int. Conf. on Fusion Energy 2008 (Geneva, Switzerland, 2008)* (Vienna: IAEA) EX/4-3Ra
[58] Gál K. *et al* 2008 Mitigation of ELMs and disruptions by pellet injection *Proc. 22nd Int. Conf. on Fusion Energy 2008 (Geneva, Switzerland, 2008)* (Vienna: IAEA) TH/P4-5
[59] Hayashi N. *et al* 2008 Integrated simulation of ELM energy loss and cycle in improved H-mode plasmas *Proc. 22nd Int. Conf. on Fusion Energy 2008 (Geneva, Switzerland, 2008)* (Vienna: IAEA) TH/P9-14
[60] Izzo V.A. *et al* 2008 RMP enhanced transport and rotation screening in DIII-D simulations *Proc. 22nd Int. Conf. on Fusion Energy 2008 (Geneva, Switzerland, 2008)* (Vienna: IAEA) TH/P4-19
[61] Liang Y. *et al* 2007 *Phys. Rev. Lett.* **98** 265004
[62] Liang Y. *et al* 2008 Active control of Type-I edge localized modes with n=1 and n=2 fields on JET *Proc. 22nd Int. Conf. on Fusion Energy 2008 (Geneva, Switzerland, 2008)* (Vienna: IAEA) EX/4-2
[63] Lang P.T. *et al* 2008 Investigating pellet physics for ELM pacing and particle fueling in ITER *Proc. 22nd Int. Conf. on Fusion Energy 2008 (Geneva, Switzerland, 2008)* (Vienna: IAEA) EX/4-5
[64] Kirk A. *et al* 2008 ELM power loading and control on MAST using resonant magnetic perturbations *Proc. 22nd Int. Conf. on Fusion Energy 2008 (Geneva, Switzerland, 2008)* (Vienna: IAEA) EX/P6-3
[65] Maingi R. *et al* 2008 Comparison of small ELM characteristics and regimes in Alcator C-Mod, MAST and NSTX *Proc. 22nd Int. Conf. on Fusion Energy 2008 (Geneva, Switzerland, 2008)* (Vienna: IAEA) EX/P6-4
[66] Sabbagh S. *et al* 2008 Advances in global MHD mode stabilization research on NSTX *Proc. 22nd Int. Conf. on Fusion Energy 2008 (Geneva, Switzerland, 2008)* (Vienna: IAEA) EX/5-1
[67] Strauss H.R. *et al* 2009 MHD simulation of resonant magnetic perturbations *Nucl. Fusion* at press
[68] Thomas P.R. *et al* 2008 ELM Physics and ELM Mitigation in ITER *Proc. 22nd Int. Conf. on Fusion Energy 2008 (Geneva, Switzerland, 2008)* (Vienna: IAEA) IT/1-5
[69] Martin Y. *et al* 2004 *Proc. 31st EPS Conf. on Plasma Physics (London, UK)* vol 28G (ECA) P4-133 http://epsppd.epfl.ch/London/pdf/P4_133.pdf
[70] Degeling A.W. *et al* 2003 *Plasma Phys. Control. Fusion* **45** 1637
[71] Romanelli F. *et al* 2009 Overview of JET results *Nucl. Fusion* at press
[72] Lang P.T. *et al* 2004 *Nucl. Fusion* **44** 665
[73] Lang P.T. *et al* 2002 *Nucl. Fusion* **42** 388
[74] Valovic M. *et al* 2008 *Nucl. Fusion* **48** 075006
[75] Mori M. *et al* 1993 *Proc. 14th Int. Conf. on Plasma Physics and Controlled Nuclear Fusion Research 1992 (Wuerzburg, 1992)* vol 2 (Vienna: IAEA) p 567

[76] Park J.-K. *et al* 2008 New understanding of tokamak plasma response to 3D magnetic fields *Proc. 22nd Int. Conf. on Fusion Energy 2008 (Geneva, Switzerland, 2008)* (Vienna: IAEA) EX/5-3Rb
[77] Park G. *et al* 2008 *Proc. 22nd Int. Conf. on Fusion Energy 2008 (Geneva, Switzerland, 2008)* (Vienna: IAEA) TH/P4-10
[78] Shaing K.C. *et al* 2008 Critical toroidal rotation profile for resistive wall modes and control of magnetic islands in tokamaks *Proc. 22nd Int. Conf. on Fusion Energy 2008 (Geneva, Switzerland, 2008)* (Vienna: IAEA) TH/P9-30
[79] Hender T.C. *et al* 2007 Progress in the ITER Physics Basis *Nucl. Fusion* **47** S128
[80] Reimerdes H. *et al* 2008 Effect of resonant and non-resonant magnetic braking on error field tolerances in high beta plasmas *Proc. 22nd Int. Conf. on Fusion Energy 2008 (Geneva, Switzerland, 2008)* (Vienna: IAEA) EX/5-3Ra
[81] Okabayashi M. *et al* 2008 Comprehensive control of resistive wall modes in DIII-D advanced tokamak plasmas *Proc. 22nd Int. Conf. on Fusion Energy 2008 (Geneva, Switzerland, 2008)* (Vienna: IAEA) EX/P9-5
[82] Sabbagh S.A. *et al* 2006 *Phys. Rev. Lett.* **97** 045004
[83] Bialek J., Boozer A.H., Mauel M.E. and Navratil G.A. 2001 *Phys. Plasmas* **8** 2170
[84] Liu Y.Q. *et al* 2006 *Phys. Plasmas* **13** 056120
[85] Sempf M., Merkel P., Strumberger E. and Guenter S. 2008 *35th EPS Conf. on Plasma Physics (Hersonissos, Greece, 9–13 June 2008)* vol 32 (ECA) P-1.077 http://epsppd.epfl.ch/Hersonissos/pdf/P1_077.pdf
[86] Connor J.W. and Hastie R.J. 1975 *Nucl. Fusion* **15** 415
[87] Rosenbluth M.N. *et al* 1997 *Nucl. Fusion* **37** 955
[88] Noll P. *et al* 1996 *Proc. 19th Symp. on Fusion Technology (Lisbon, Portugal, 1996)* vol 1 (Amsterdam: Elsevier) p 751
[89] Riccardo V., Noll P. and Walker S.P. 2000 *Nucl. Fusion* **40** 1805
[90] Zakharov L. 2008 *Phys. Plasmas* **15** 062507
[91] Arnoux G. *et al* 2008 Heat loads on plasma facing components during disruptions on JET *Proc. 22nd Int. Conf. on Fusion Energy 2008 (Geneva, Switzerland, 2008)* (Vienna: IAEA) EX/7-2Ra
[92] Bandyopadhy I. *et al* 2008 Simulations of ITER disruptions and VDE scenarios with TSC and comparison with DINA results *Proc. 22nd Int. Conf. on Fusion Energy 2008 (Geneva, Switzerland, 2008)* (Vienna: IAEA) IT/P6-17
[93] Esposito B. *et al* 2009 Disruption control on FTU and ASDEX Upgrade with ECRH *Nucl. Fusion* at press
[94] Pokol G. *et al* 2008 Criteria for runaway electron generation in tokamak disruptions *Proc. 22nd Int. Conf. on Fusion Energy 2008 (Geneva, Switzerland, 2008)* (Vienna: IAEA) TH/P3-4
[95] Okamoto V. *et al* 2008 Study of current decay time during disruptions in JT-60U tokamak *Proc. 22nd Int. Conf. on Fusion Energy 2008 (Geneva, Switzerland, 2008)* (Vienna: IAEA) EX/7-2Rc
[96] Riccardo V. *et al* 2008 *Proc. 22nd Int. Conf. on Fusion Energy 2008 (Geneva, Switzerland, 2008)* (Vienna: IAEA) EX/7-2Rb
[97] Savrukin P.V. *et al* 2008 Effect of the MHD perturbations on runaway beam formation during disruptions in the T-10 tokamak *Proc. 22nd Int. Conf. on Fusion Energy 2008 (Geneva, Switzerland, 2008)* (Vienna: IAEA) EX/7-3Rc
[98] Wesley J.C. *et al* 2008 Fast plasma shutdowns obtained with massive hydrogenic, noble and mixed-gas injection in DIII-D *Proc. 22nd Int. Conf. on Fusion Energy 2008 (Geneva, Switzerland, 2008)* (Vienna: IAEA) EX/7-3Rb
[99] Whyte D.G. *et al* 2008 Studies of requirements for ITER disruption mitigation systems *Proc. 22nd Int. Conf. on Fusion Energy 2008 (Geneva, Switzerland, 2008)* (Vienna: IAEA) IT/P6-18
[100] Pautasso G. *et al* 2008 Disruption mitigation in ASDEX Upgrade with the in-vessel fast valve *Proc. 22nd Int. Conf. on Fusion Energy 2008 (Geneva, Switzerland, 2008)* (Vienna: IAEA) EX/P9-1